Transient Stability of Power in DFIG Wind Farm through Resilient with AFRR, IDA-PBC and PID Control

TADJEDDINE Ali Abderrazak[*1], Arbaoui Iliace[2], Bendelhoum Mohamed Sofiane[1], Bendjillali Ridha Ilyas[1], Hamiani Hichem[1],

[1]LSETER Laboratory, Technology Institute, University Center Nour Bachir, El-Bayadh, Algeria
[2]Faculty of Science and Technology University of Adrar, Algeria,

[*]Corresponding author; Email: atadj1@gmail.com

Article Info

Article history:

Received , 04/09/2023
Revised , 23/09/2023
Accepted , 20/10/2023

Keywords:

IDA-PBC,
Renewable Energy Integration,
Dynamic ZIP Load,
DFIG Wind turbine,
PIAT grid stability.

ABSTRACT

This work addresses the integration challenges of Variable Renewable Energy (VRE) sources within the Kabertene wind farm and photovoltaic systems in Adrar, Algeria. Fluctuations in electricity consumption and the impact of weather conditions on power generation raise stability concerns for the southern PIAT grid. The PIAT grid includes distributed generation units, a wind farm, photovoltaic parks, dynamic RLC lines, and nonlinear D-ZIP loads. To ensure high power quality across the PIAT network, advanced control methods are developed, using IDA-PBC passivity theory and PID controllers for Kabertene's VRE components DFIGs and PVs. An Automatic Frequency Restoration Reserve (AFRR) is employed to stabilize frequency and voltages on the PIAT grid. A decentralized control approach is proposed, building on decentralized multivariable PID controllers, effectively managing voltage stability in generation units and dynamic loads. Simulation and analysis demonstrate the effectiveness of these techniques in enhancing grid stability, minimizing frequency deviations, and simplifying VRE integration. Practical implementation aspects are highlighted, emphasizing the transition to a cleaner, more sustainable energy system.

I. Introduction

The incorporation of Variable Renewable Energy (VRE), like solar and wind, into power grids signifies a significant move towards sustainability. Yet, this integration poses notable technical obstacles, primarily due to the fluctuating and intermittent nature of VRE sources. Unlike traditional coal or gas sources, VRE outputs are subject to weather-induced changes, like varying sunlight or wind speeds [1].

Harnessing Renewable Energy Sources (RES), is crucial in tackling contemporary environmental challenges including climate change, pollution, and biodiversity loss attributed to fossil fuel consumption [2]. Renewable energy offers a cleaner, more sustainable alternative, reducing dependence on finite resources and minimizing environmental harm [3]-[4].

Sustaining a reliable supply-demand equilibrium within electrical grids necessitates stability. Achieving this equilibrium involves integrating energy storage systems such as batteries or pumped hydro storage. These systems store surplus energy during peak generation times and release it during low-output periods, ensuring grid stability. Beyond energy storage, advanced control technologies as demand response and smart grids play a pivotal role in

VRE integration [5]. These technologies enable real-time management and grid balancing, effectively mitigating challenges arising from VRE source variability [6].

In a separate context, the isolated PIAT power network in southern Algeria, depicted in Figure 1, functions autonomously from the national grid. It generates and distributes locally sourced renewable energy, predominantly solar and wind. Anticipated to contribute 18.67% of variable renewable energy (VRE) to the energy mix in 2023, this network addresses 153 GWh of annual energy demand [7]. This integration signifies a reduction in carbon footprint and a stride towards sustainability. PIAT's development is instrumental in Algeria's pursuit of an environmentally friendly energy paradigm, utilizing regional renewable resources to mitigate emissions, preserve nature, and enhance local energy access. Wind turbines are crucial contributors to renewable energy, offering eco-friendly electricity generation [8]-[9]. However, their impact on power system stability raises integration concerns. Addressing challenges like reactive power support under unbalanced voltage conditions is essential for reliable grid contribution [10].

A significant issue is wind turbine vulnerability during grid failures, especially in Doubly Fed Induction Generators (DFIG) systems where grid connectivity affects the generator. This susceptibility causes voltage fluctuations and grid instability, demanding effective control strategies to ensure secure operation amid various grid scenarios [11].

DFIG systems face rotor winding vulnerability to over-voltage and over-current from negative sequence voltage. Increased slip due to negative sequence voltage leads to rotor winding damage, undermining turbine reliability and efficiency [12]-[13].

DFIGs, a common wind turbine type, offer variable speed operation and efficient power conversion. Despite introducing stability issues during transient disturbances, DFIGs enhance wind power systems by boosting efficiency, stability, and performance [14]. Their adaptability to variable speeds optimizes wind energy capture while reducing power electronics size and cost for grid compatibility. Incorporating non-linear load models considering diverse consumption patterns is vital. This aids operators in efficiently managing the electrical grid in the Pole InSalah-Adrar-Timimoune (PIAT) region.

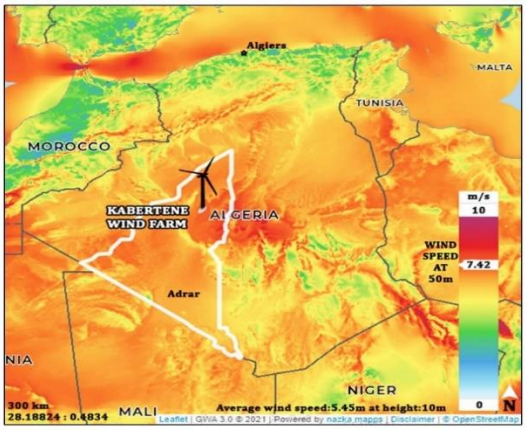

Figure 1. Wind Potential in Adrar region, Algeria

DFIG generators offer a crucial advantage in their ability to regulate rotor speed, enabling precise power generation control. Achieved through a power electronics converter, this control includes frequency, reactive power, and voltage regulation. Rotor speed control ensures a steady output frequency, vital for efficient and stable grid operation [15]-[20].

IDA-PBC control technique guarantees system stability and robustness. Implementing it in DFIG wind turbines demands a suitable Lyapunov function ensuring system passivity, and a controller meeting control goals. Objectives include boosting energy efficiency, cost reduction, minimizing MW and MVar losses, and optimizing shunt var devices. Constraints encompass physical limitations like rotor speed or DC-link voltage [21]-[27].

Managing asynchronous generators in variable-speed drives is intricate due to their intricate nature. These drives possess a multivariable, nonlinear mathematical model, with a strong interdependency between magnetic flux and electromagnetic torque control parameters [28]. Conventional linear regulators are inadequate, requiring robust, computationally efficient advanced regulators, particularly given the high system speed. Nonlinear system control is a growing research field, with various approaches described in literature for achieving robust control [29]-[31]. Figure 2 illustrates geographical maps displaying the locations of renewable energy installations within the Kabertene Photovoltaic and Wind farm parks situated in the southern region of Algeria.

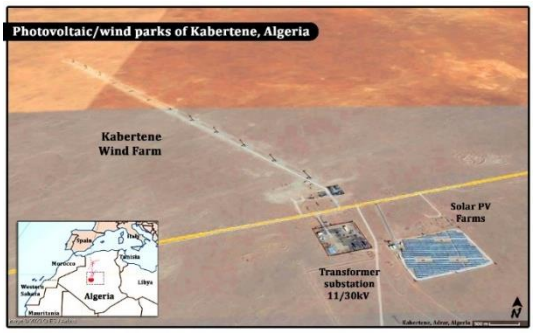

Figure 2. Maps geographic Kabertene PV/WF parks in Algeria

With the increasing adoption of solar and wind power in the PIAT grid, maintaining frequency control gains paramount importance. Regional wind speeds average between 3 to 5 m/s. However, the intermittent nature of these renewable sources poses distinct challenges in preserving a consistent system frequency. Efforts to ensure frequency control in Variable Renewable Energy (VRE) systems pivot on balancing electricity supply and demand. Surplus renewable generation can elevate frequency, risking instability, while inadequate generation causes frequency drops. Thus, effective frequency control becomes pivotal to averting deviations and ensuring grid stability.

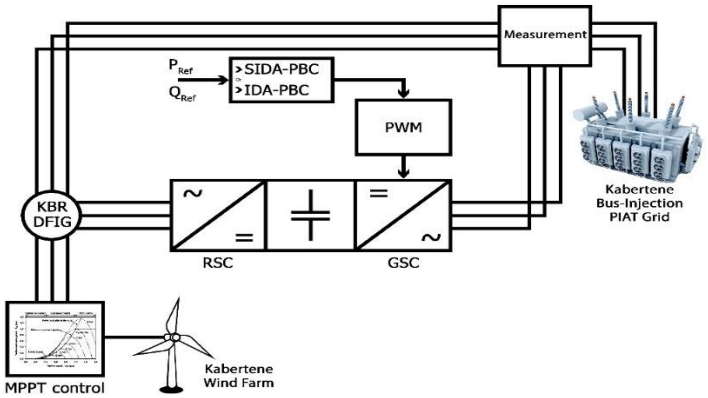

Figure 3. Block diagram of wind DFIG structure with MPPT, SIDA-PBC and IDA-PBC control

Our study centers on active and reactive power production, integration, and power flow analysis utilizing the passive control mathematical model. We assess its efficacy in attaining set objectives, focusing on the PIAT grid, particularly the Kabertene Wind Farm in southern Algeria, with a 10.2 MW capacity. Our findings reveal the control system's notable success in regulating the DFIG's active and reactive power outputs. Moreover, the incorporation of a Power System Stabilizer (PSS) significantly enhances power system stability, especially during disturbances [32]-[36].

Figure 4 displays the one-line diagram depicting the Kabertene Photovoltaic (PV) segment within the Pole InSalah-Adrar-Timimoune (PIAT) electrical grid.

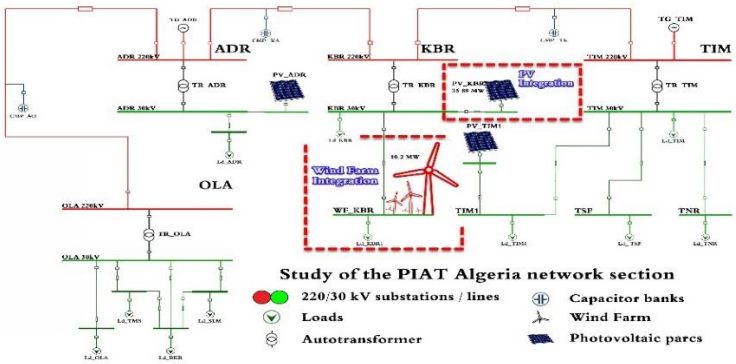

Figure 4. Kabertene PV/WF section study of PIAT electrical grid

The study provides valuable insights into the formulation of control systems tailored for the utilization of Doubly Fed Induction Generators (DFIGs) within wind farms. The proposed Inner-Droop control scheme in conjunction with the Input-to-State Stability (ISS) Passivity-Based Control (PBC) strategy offers several noteworthy advantages [37]. These include an elevated transient response and a robustness against uncertainties stemming from wind speed variations [38]-[42]. The paper furnishes a comprehensive analysis of the intricacies inherent in control system development for DFIGs, underscoring the paramount importance of stability in ensuring the dependable operation of wind farms [43]. This acquired knowledge assumes a pivotal role in safeguarding the reliability, stability, and optimal efficiency of electrical grids. The overarching formulation of the ZIP model can be succinctly expressed as follows:

$$\begin{cases} P = P_0\left[a_p\left(\frac{V}{V_0}\right)^2 + b_p\left(\frac{V}{V_0}\right) + c_p\right]\left[1 - k_{pf}\Delta f\right] \\ Q = Q_0\left[a_q\left(\frac{V}{V_0}\right)^2 + b_q\left(\frac{V}{V_0}\right) + c_q\right]\left[1 - k_{qf}\Delta f\right] \end{cases} \quad (1)$$

In these equations:

P and Q represent the active and reactive powers of the load for the operating voltage V,

P_0 and Q_0 denote the active and reactive powers of the load for the nominal voltage V_0,

a_p, b_p, c_p, a_q, b_q, and c_q are the coefficients of the ZIP model,

k_{pf} is the sensitivity parameter of the active power, typically ranging from 0 to 3,

k_{qf} is the sensitivity parameter of the reactive power, typically ranging from -2 to 0,

Δf represents the frequency deviation in P.u.

II. Research Method

II.1. Wind turbine PCH modeling

The equation of wind power is:

$$P_v = \frac{1}{2}\sigma.S.v^3 \quad (2)$$

σ : Density of the air.

S : Turbine circular surface.

v : wind speed.

The aerodynamic power of the turbine is then written:

$$P_{aero} = C_p.P_v = C_p(\lambda,\beta)\frac{1}{2}\rho.S.v^3 \quad (3)$$

ϑ The specific speed:

$$\vartheta = \frac{R\Omega_{wind}}{v}$$

The coefficient of aerodynamic power C_p of the wind turbine:

$$C_p(\lambda,\beta) = C_1\left(C_2\frac{1}{\Lambda} - C_3\beta^x - C_4 - C_5\right)e^{\frac{-C_6}{\Lambda}} \quad (4)$$

Knowing that:

$$\frac{1}{\Lambda} = \left(\frac{1}{\lambda+0.08\beta} - \frac{0.035}{1+\beta^3}\right) \quad (5)$$

The torque of the wind turbine is given by:

$$T_{mec} = \frac{P_{mec}}{w} = \frac{1}{2}\frac{\rho.S.v^3C_p(\lambda,\beta)}{w} \quad (6)$$

The mechanical speed from the total mechanical torque T_{mec} applied to the rotor:

$$J\frac{d\Omega_{mec}}{dt} = T_{mec} \tag{7}$$

J : Total inertia appears in the generator rotor.

$$J = \frac{J_{turbine}}{G} + J_{DFIG} \tag{8}$$

In an academic context, the mechanical torque T_{mec} incorporates the electromagnetic torque T_{em} generated by the generator, the torque resulting from viscous friction T_{vis}, and the torque originating from the gearbox T_g.

$$T_{mec} = T_g - T_{em} - T_{vis} \tag{9}$$

II.2. DFIG PCH model

The model of the double-feed generator in the d-q reference can be written as below [3, 4]:

$$\begin{cases} V_{ds} = R_s I_{ds} + \frac{d\Phi_{ds}}{dt} - \omega_s \Phi_{qs} \\ V_{qs} = R_s I_{qs} + \frac{d\Phi_{qs}}{dt} + \omega_s \Phi_{ds} \\ V_{dr} = R_r I_{dr} + \frac{d\Phi_{dr}}{dt} - (\omega_s - \omega)\Phi_{qr} \\ V_{qr} = R_r I_{qr} + \frac{d\Phi_{qr}}{dt} + (\omega_s - \omega)\Phi_{dr} \\ J\frac{d\omega}{dt} = M\left(I_{dr}I_{qs} - I_{ds}I_{qr}\right) - C_r - C_f\omega \end{cases} \tag{10}$$

We obtain by way of using the flow equations 4 and 6:

$$\begin{aligned} \dot{\Phi}_{ds} &= V_{ds} - R_s I_{ds} + \omega_s L_s I_{qs} + \omega_s M I_{qr} \\ \dot{\Phi}_{qs} &= V_{qs} - R_s I_{qs} - \omega_s L_s I_{ds} - \omega_s M I_{dr} \\ \dot{\Phi}_{dr} &= V_{dr} - R_r I_{dr} + (\omega_s - \omega) L_r I_{qr} + (\omega_s - \omega) M I_{qs} \\ \dot{\Phi}_{qr} &= V_{qr} - R_r I_{qr} - (\omega_s - \omega) L_r I_{dr} - (\omega_s - \omega) M I_{ds} \end{aligned} \tag{11}$$

Where:

$$\dot{\Phi}_s = V_s - R_s I_2 I_s - \omega_s L_s J_2 I_s - \omega_s M J_2 I_r \tag{12}$$

$$\dot{\Phi}_r = V_r - R_r I_2 I_r - (\omega_s - \omega) M J_2 I_s - (\omega_s - \omega) L_r J_2 I_r \tag{13}$$

And, $J_{DFIG}\frac{d\omega}{dt} = L_{sr} I_s^T J_2 I_r - C_r - C_f\omega$ (14)

With:

$$\Phi_s = \begin{bmatrix} \Phi_{ds} \\ \Phi_{qs} \end{bmatrix}, \Phi_r = \begin{bmatrix} \Phi_{dr} \\ \Phi_{qr} \end{bmatrix},$$

$$I_s = \begin{bmatrix} I_{ds} \\ I_{qs} \end{bmatrix}, I_r = \begin{bmatrix} I_{dr} \\ I_{qr} \end{bmatrix}, I_2 = \begin{bmatrix} 1 & 0 \\ 0 & 1 \end{bmatrix}, J_2 = \begin{bmatrix} 0 & -1 \\ 1 & 0 \end{bmatrix}$$

The state variables are:

$$x = \left[{\Phi_s}^T, {\Phi_r}^T, J_{DFIG}\omega\right]^T = [x_e^T, x_m]^T$$

With:

$x_e^T = \left[{\Phi_s}^T, {\Phi_r}^T\right]$: are the electrical state variables.

$x_m = J_{DFIG}\omega$: Mechanical variable.

The energy function written by:

$$H(x) = \frac{1}{2}x_e^T L^{-1} x_e + \frac{1}{2J_{DFIG}}x_m^2 \tag{15}$$

With:

$$L = \begin{bmatrix} L_s I_2 & M I_2 \\ M I_2 & L_r I_2 \end{bmatrix}$$

Regarding the state variables, the energy can be partially differentiated with respect to the following variables:

$$\begin{cases} \frac{\partial H}{\partial x_e} = L^{-1}x_e \\ \frac{\partial H}{\partial x_m} = J_{DFIG}^{-1}x_m \end{cases} \Rightarrow \begin{cases} \frac{\partial H}{\partial x_e} = L^{-1}x_e = I = [I_s^T, I_r^T]^T \\ \frac{\partial H}{\partial x_m} = J_{DFIG}^{-1}x_m = \omega \end{cases} \quad (16)$$

The control matrices:

$$J(x) = \begin{bmatrix} -\omega_s L_s J_2 & -\omega_s M J_2 & 0_{2\times1} \\ -\omega_s L_s J_2 & -(\omega_s - \omega) L_s J_2 & M J_2 I_s \\ 0_{1\times2} & M I_s^T J_2 & 0 \end{bmatrix}$$

$$R(x) = \begin{bmatrix} R_s I_2 & 0_{2\times2} & 0_{2\times1} \\ 0_{2\times2} & R_r I_2 & 0_{2\times1} \\ 0_{1\times2} & 0_{1\times2} & C_f \end{bmatrix}$$

$$g(x) = \begin{bmatrix} I_2 & 0_{2\times2} & 0_{2\times1} \\ 0_{2\times2} & I_2 & 0_{2\times1} \\ 0_{1\times2} & 0_{1\times2} & 1 \end{bmatrix}, u = [V_s^T \quad V_r^T \quad T_r]^T$$

With:

$0_{2\times2} = \begin{bmatrix} 0 & 0 \\ 0 & 0 \end{bmatrix}$, $0_{2\times1} = \begin{bmatrix} 0 \\ 0 \end{bmatrix}$, $0_{1\times2} = [0 \quad 0]$,

$J(x) = J(x)^{-1}$, $R(x) = R(x)^T \geq 0$

Finally, the interconnection, depreciation and control matrices are:

$$\begin{cases} \dot{x} = \left[\begin{bmatrix} -\omega_s L_s J_2 & -\omega_s M J_2 & 0_{2\times1} \\ -\omega_s M J_2 & -(\omega_s - \omega) L_s J_2 & M J_2 I_s \\ 0_{1\times2} & M I_s^T J_2 & 0 \end{bmatrix} - \begin{bmatrix} R_s I_2 & 0_{2\times2} & 0_{2\times1} \\ 0_{2\times2} & R_r I_2 & 0_{2\times1} \\ 0_{1\times2} & 0_{1\times2} & T_f \end{bmatrix} \right] \nabla H + \begin{bmatrix} I_2 & 0_{2\times2} & 0_{2\times1} \\ 0_{2\times2} & I_2 & 0_{2\times1} \\ 0_{1\times2} & 0_{1\times2} & 1 \end{bmatrix} \begin{bmatrix} V_s^T \\ V_r^T \\ T_r \end{bmatrix} \\ \dot{y} = \begin{bmatrix} I_2 & 0_{2\times2} & 0_{2\times1} \\ 0_{2\times2} & I_2 & 0_{2\times1} \\ 0_{1\times2} & 0_{1\times2} & 1 \end{bmatrix} \nabla H \end{cases} \quad (17)$$

II.3. IDA-PBC control of the wind system

From the equation (10), it is clear that the dynamic model of the DFIG is non-linear due to the coupling between the speed and the electric currents. According to the vector control principle, the direct axis current Id is always forced to equal zero in order to orient all the linkage flux in the d axis and achieve maximum torque per ampere.

$$\begin{cases} \frac{d\Phi_{ds}}{dt} = V_{ds} - R_s I_{ds} + \omega_s L_s I_{qs} + \omega_s M I_{qr} \\ \frac{d\Phi_{qs}}{dt} = V_{qs} - R_s I_{qs} - \omega_s L_s I_{ds} - \omega_s M I_{dr} \\ \frac{d\Phi_{dr}}{dt} = V_{dr} - R_r I_{dr} + \omega_r L_r I_{qr} + \omega_r M I_{qs} \\ \frac{d\Phi_{qr}}{dt} = V_{qr} - R_r I_{qr} - \omega_r L_r I_{dr} + \omega_r M I_{ds} \end{cases} \quad (18)$$

So the mechanical equation of the rotating part of the generator is given by:

$$J\frac{d\omega}{dt} = M I_s^T J_2 I_r - T_r - T_f \quad (19)$$

Where; $J_2 = \begin{bmatrix} 0 & -1 \\ 1 & 0 \end{bmatrix}$, $I_s = \begin{bmatrix} I_{ds} \\ I_{qs} \end{bmatrix}$, $I_r = \begin{bmatrix} I_{dr} \\ I_{qr} \end{bmatrix}$

The state variables are:

$x = [\Phi_s^T \quad \Phi_r^T \quad J\omega]^T = [x_e^T \quad x_m]^T$

With:

$x_e^T = [\Phi_s^T \quad \Phi_r^T]$: are the electric state variables.

$x_m = J\omega$: Mechanical variable.

The energy function written by:

$$H(x) = \frac{1}{2}x_e^T L^{-1} x_e + \frac{1}{2J_{DFIG}}x_m^2 \tag{20}$$

With: $= \begin{bmatrix} L_s I_2 & MI_2 \\ MI_2 & L_r I_2 \end{bmatrix}$, $I_2 = \begin{bmatrix} 1 & 0 \\ 0 & 1 \end{bmatrix}$

The partial derivatives of energy with respect to the state variables are:

$$\begin{cases} \frac{\partial H}{\partial x_e} = L^{-1}x_e \\ \frac{\partial H}{\partial x_m} = J^{-1}x_m \end{cases} \Rightarrow \begin{cases} \frac{\partial H}{\partial x_e} = I = [I_s^T \quad I_r^T]^T \\ \frac{\partial H}{\partial x_m} = \omega \end{cases} \tag{21}$$

Finally, the matrices of interconnection, damping and the matrix of the command are:

$$J(x) = \begin{bmatrix} -\omega_s L_s J_2 & -\omega_s M J_2 & 0_{2\times 1} \\ -\omega_s L_s J_2 & -\omega_r L_s J_2 & MJ_2 I_s \\ 0_{1\times 2} & MI_s^T J_2 & 0 \end{bmatrix}, \; R(x) = \begin{bmatrix} R_s I_2 & 0_{2\times 2} & 0_{2\times 1} \\ 0_{2\times 2} & R_r I_2 & 0_{2\times 1} \\ 0_{1\times 2} & 0_{1\times 2} & T_f \end{bmatrix} \tag{22}$$

$$\mathrm{g}(x) = \begin{bmatrix} I_2 & 0_{2\times 2} & 0_{2\times 1} \\ 0_{2\times 2} & I_2 & 0_{2\times 1} \\ 0_{1\times 2} & 0_{1\times 2} & 1 \end{bmatrix}, u = [V_s^T \quad V_r^T \quad T_r]^T \tag{23}$$

With:

$$0_{2\times 2} = \begin{bmatrix} 0 & 0 \\ 0 & 0 \end{bmatrix}, 0_{2\times 1} = \begin{bmatrix} 0 \\ 0 \end{bmatrix}, 0_{1\times 2} = [0 \quad 0], V_s^T = \begin{bmatrix} V_{ds} \\ V_{qs} \end{bmatrix}, V_r^T = \begin{bmatrix} V_{dr} \\ V_{qr} \end{bmatrix}$$

$$J(x) = J(x)^{-1}, R(x) = R(x)^T \geq 0 \tag{24}$$

With these matrices the model PCH is written by:

$$\begin{cases} \dot{x} = \left[\begin{bmatrix} -\omega_s L_s J_2 & -\omega_s M J_2 & 0_{2\times 1} \\ -\omega_s M J_2 & -\omega_r L_s J_2 & M J_2 I_s \\ 0_{1\times 2} & M I_s^T J_2 & 0 \end{bmatrix} - \begin{bmatrix} R_s I_2 & 0_{2\times 2} & 0_{2\times 1} \\ 0_{2\times 2} & R_r I_2 & 0_{2\times 1} \\ 0_{1\times 2} & 0_{1\times 2} & T_f \end{bmatrix} \right] \nabla H + \begin{bmatrix} I_2 & 0_{2\times 2} & 0_{2\times 1} \\ 0_{2\times 2} & I_2 & 0_{2\times 1} \\ 0_{1\times 2} & 0_{1\times 2} & 1 \end{bmatrix} \begin{bmatrix} V_s^T \\ V_r^T \\ T_r \end{bmatrix} \\ \dot{y} = \begin{bmatrix} I_2 & 0_{2\times 2} & 0_{2\times 1} \\ 0_{2\times 2} & I_2 & 0_{2\times 1} \\ 0_{1\times 2} & 0_{1\times 2} & 1 \end{bmatrix} \nabla H \end{cases} \tag{25}$$

II.4. Calculation of control voltages V_{dr}, V_{qr}

To calculate the control voltages one has to determine $J_d(x)$ and $R_d(x)$

For that we must determine $J_a(x)$, $R_a(x)$ the controller. The closed-loop system is written by:

$$f(x) + \mathrm{g}(x)u = \big(J_d(x) - R_d(x)\big)\partial H_d(x) \tag{26}$$

Where:

$J_d(x) = J(x) + J_a(x)$

$R_d(x) = R(x) + R_a(x)$

$H_d(x) = H(x) + H_a(x)$

With:

$H_d(x)$: The energy function of the closed-loop system, $H_a(x)$: The controller energy function.

$J_d(x)$: The interconnection matrix of the closed-loop system, $J_a(x)$: The controller interconnection matrix.

$R_d(x)$: The damping matrix of the closed-loop system, $R_a(x)$: The controller damping matrix

It is possible to write equation (26) as follows:

$$\big(J(x)+J_a(x)-R(x)+R_a(x)\big)\partial H_d(x)=-\big(J_a(x)-R_a(x)\big)\partial H(x)+\mathrm{g}(x)u \tag{27}$$

The previous equation is equivalent to:

$$\big(J_d(x)-R_d(x)\big)\partial H_a(x)=-\big(J_a(x)-R_a(x)\big)\partial H(x)+\mathrm{g}(x)u \tag{28}$$

So the total energy desired:

$$H_d(x)=\frac{1}{2}(x_e-x_e^*)^T L^{-1}(x_e-x_e^*)+\frac{1}{2J_{DFIG}}(x_m-x_m^*)^2 \tag{29}$$

So: $H_a(x)=H_d(x)-H(x)=-x_e^T L^{-1}x_e-\frac{1}{J_{DFIG}}x_m^* x_m+\frac{1}{2}x_e^{*T}L^{-1}x_e^*+\frac{1}{2J_{DFIG}}x_e^{*2}$ (30)

With: $H_a(x)=\begin{bmatrix}-I^*\\-\omega^*\end{bmatrix}$, where $I=[I_{ds}\quad I_{qs}\quad I_{dr}\quad I_{qr}]^T$

Using this relationship, equation (30) becomes:

$$\big(J_d(x)-R_d(x)\big)\begin{bmatrix}-I^*\\-\omega^*\end{bmatrix}=-\big(J_a(x)-R_a(x)\big)\begin{bmatrix}I\\\omega\end{bmatrix}+g(x)u \tag{31}$$

The command Vr is found in line 3 and 4 of the matrix equation (31).

$$\text{So: }\begin{cases}J_a(x)=\begin{bmatrix}0_{2\times2}&0_{2\times2}&0_{2\times1}\\0_{2\times2}&0_{2\times2}&-J_{rm}(x)\\0_{1\times2}&J_{rm}^T(x)&0\end{bmatrix}\\ R_a(x)=\begin{bmatrix}0_{2\times2}&0_{2\times2}&0_{2\times1}\\0_{2\times2}&rI_2&0_{2\times1}\\0_{1\times2}&0_{1\times2}&0\end{bmatrix}\end{cases} \tag{32}$$

Where: $J_{rm}(x)\in\Re^{2\times1}$ to be determined.

r : It is an additional resistance for currents to dampen transient oscillations.

We replace the matrices $J_a(x)$,$R_a(x)$ and using equation (32), we find:

$$J_{rm}^T(x)=M\frac{(I_r-I_r^*)^T}{|I_r-I_r^*|^2}(I_s-I_s^*)^T J_2 I_r^* \tag{33}$$

So: $V_r=V_r^*-(\omega-\omega^*)\big(L_r J_2 I_r^*+J_{rm}(x)\big)-M\omega^* J_2(I_s-I_s^*)-rI_2(I_r-I_r^*)$ (34)

Unfortunately, the order is singular in point of equilibrium. It's done possible to get rid of this singularity by adding a depreciation variable. Now we keep $J_d(x)$ and $H_d(x)$ as before, and we change the matrix to have the form:

$$R_a(x)=\begin{bmatrix}0_{2\times2}&0_{2\times2}&0_{2\times1}\\0_{2\times2}&rI_2&0_{2\times1}\\0_{1\times2}&0_{1\times2}&\xi(x)\end{bmatrix} \tag{35}$$

With: $\xi(x)=\frac{T_{em}^*-T_{em}(x_e)}{\omega-\omega^*}$ (36)

and: $T_{em}^*=C_f\omega^*$ (37)

When replaced in the closed-loop Hamiltonian equation, $\xi(x)$ is multiplied by $(\omega-\omega^*)$, therefore elimination of singularity. Since the mechanical part of (27) is the only one that has been modified, then the expression of V_r in terms of $J_{rm}(x)$ rest the same.

Using the equilibrium equations, we obtain:

$$J_{rm}(x)=MJ_2 I_s \tag{38}$$

The closed-loop dynamic system is always of the form (38) with:

$$J_d(x)=\begin{bmatrix}-\omega_s L_s J_2&-\omega_s M J_2&0_{2\times1}\\-\omega_s M J_2&-\omega_r L_s J_2&MJ_2 I_s\\0_{1\times2}&MI_s^T J_2&0\end{bmatrix};\ R_d(x)=\begin{bmatrix}R_s I_2&0_{2\times2}&0_{2\times1}\\0_{2\times2}&(R_r+r)I_2&0_{2\times1}\\0_{1\times2}&0_{1\times2}&T_f+\xi(x)\end{bmatrix} \tag{39}$$

Finally, the rotor voltages of the order are written by:

$$V_r=V_r^*-(\omega-\omega^*)(L_r J_2 I_r^*+MJ_2 I_s)-M\omega^* J_2(I_s-I_s^*)-rI_2(I_r-I_r^*) \tag{40}$$

With: $V_r^*=(\omega_s-\omega^*)(L_r J_2 I_r^*+MJ_2 I_s)+R_r I_2 I_r^*$ (41)

III. Results

Ensuring the stability of the PIAT grid is paramount to its equilibrium maintenance and swift restoration post internal or external disturbances. Achieving this stability necessitates the implementation of control and protection mechanisms, such as voltage regulators and Automatic Frequency Restoration Reserve (AFRR) systems. These devices ensure the harmony between generation and consumption while guaranteeing secure and efficient grid operation. Our research focused on the 220KV transmission network and the 60KV distribution system within the PIAT grid, located in Adrar province, southern Algeria, as depicted in Figures 5 and 6. MATLAB 2021a and ETAP 2019 were employed as software tools for result analysis and representation. To maintain voltage levels, real-time dynamic voltage violations at buses were meticulously monitored.

III.1. Frequency and voltage grid result

Figure 5 depicts the temporal evolution of the synchronism frequency correction, designated as f_r, at the integration point of Kabertene (bus 4), in conjunction with the frequency prediction model denoted as f_p. The graph visually captures the dynamic progression of the f_{OPF} value, representing the sought frequency correction for optimal synchronism, over a time duration, guided by forecasts generated by the $f_p$model. By undertaking a comparative analysis between the projected frequency f_p and the actual frequency, the model computes the appropriate f_{OPF} value, pivotal in achieving synchronization and bolstering stability within the system.

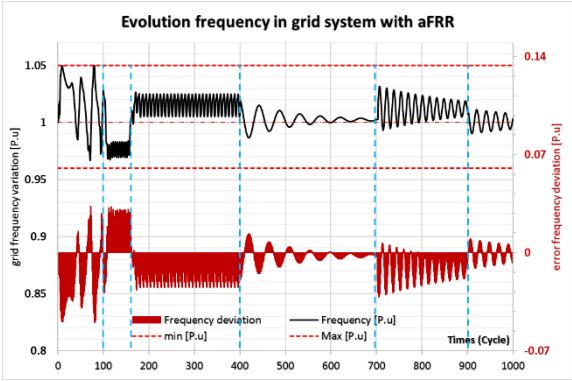

Figure 5. Frequency grid evolution with aFRR correction

The graphical representation in Figure 6 showcases the highest voltage levels documented at both the 220KV transmission and 30KV distribution buses. This evaluation considers the application of frequency control strategies both with and without the presence of Photovoltaic (PV) sources. The graph delineates the pinnacle voltage values recorded throughout the operational period of the electrical system.

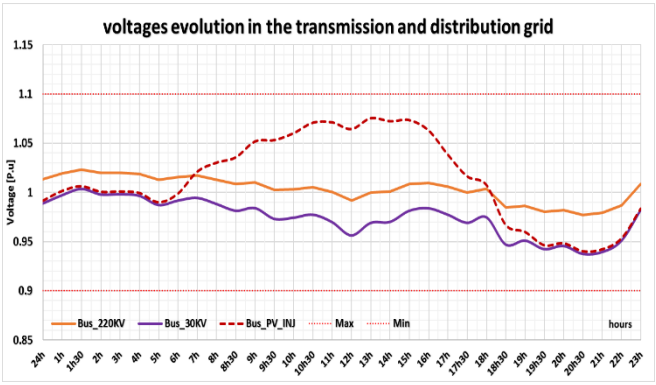

Figure 6. Voltages evolution in the 220KV transmission and 30KV distribution with PV injection bus.

The deployment of frequency control mechanisms serves the purpose of upholding voltage stability despite the inherent power generation fluctuations from Variable Renewable Energy (VRE) sources. These mechanisms proactively regulate power generation and consumption to uphold voltage levels within permissible thresholds. The graph serves as a valuable visual aid, shedding light on the influence of VRE integration on voltage levels,

and concurrently, it illustrates the efficacy of frequency control strategies in steering voltage stability management.

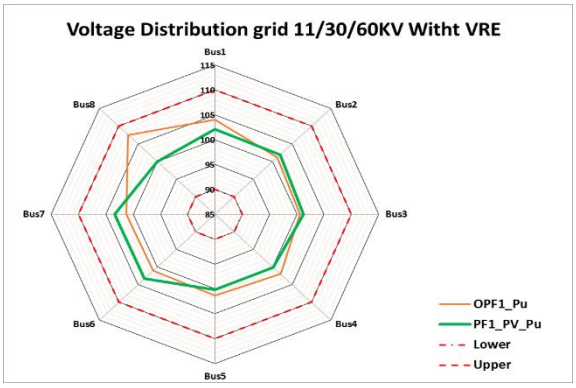

Figure 7. Maximum voltages in the 220KV transmission and 30KV distribution with VRE sources

III.2. DFIG Results

To evaluate the robustness of the Doubly Fed Induction Generator (DFIG), a customary approach involves introducing variations in the internal resistance parameter and subsequently scrutinizing the response of the applied control methodologies. Crucial metrics, including stability, transient response, power efficiency, and other pertinent performance indicators, merit thorough examination. In the specific context outlined, Figures 8, 9, and 10 are employed to present the outcomes of robustness concerning the Input-to-State Stability Passivity-Based Control (IDA-PBC) technique. These figures illustrate the impact of varying weather conditions and electrical loads (D-ZIP) on the DFIG's internal resistance and inductance values, thereby showcasing the method's resilience under these influences.

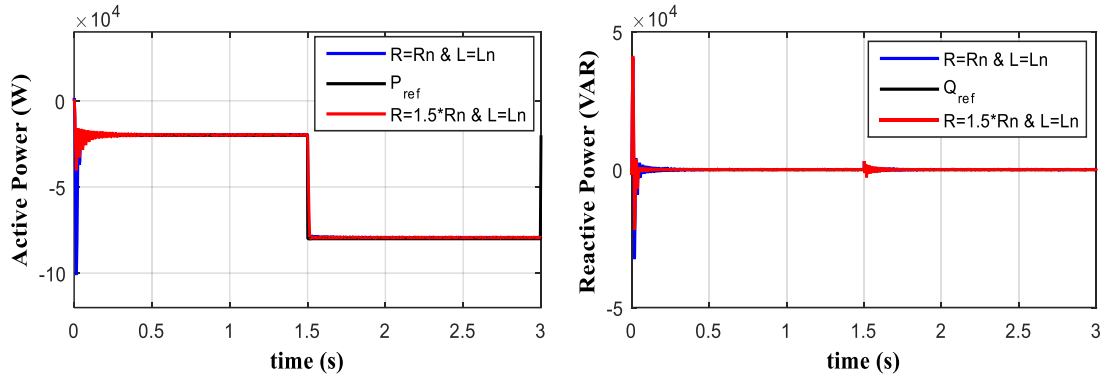

Figure 8. Effect of variations in internal resistances on the P_G & Q_G powers of the DFIG with IDA-PBC method

Figure 9 displays the outcomes highlighting the robustness of the Input-to-State Stability Passivity-Based Control (IDA PBC) methods against variations in the inductance value of the Doubly Fed Induction Generator (DFIG).

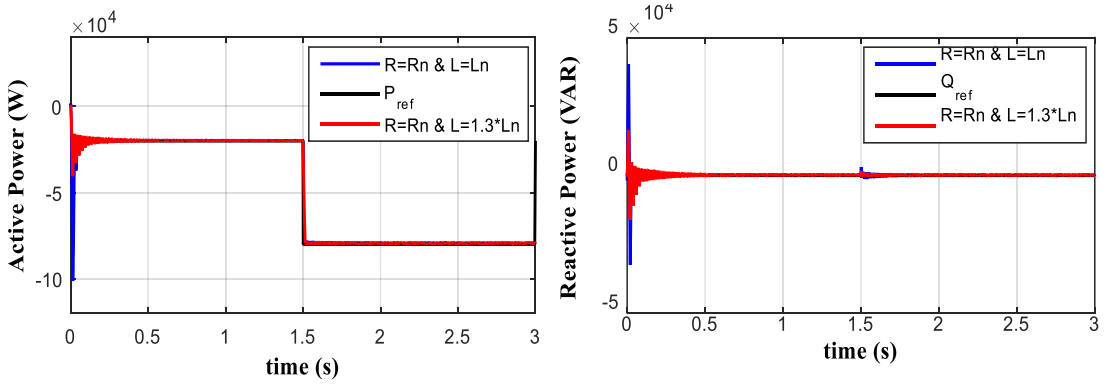

Figure 9. Effect of variations in internal inductance on the P_G & Q_G powers of the DFIG with IDA-PBC method

The results obtained for the IDA-PBC and SIDA-PBC control for MW and Mvar production is presented in the following figure 10.

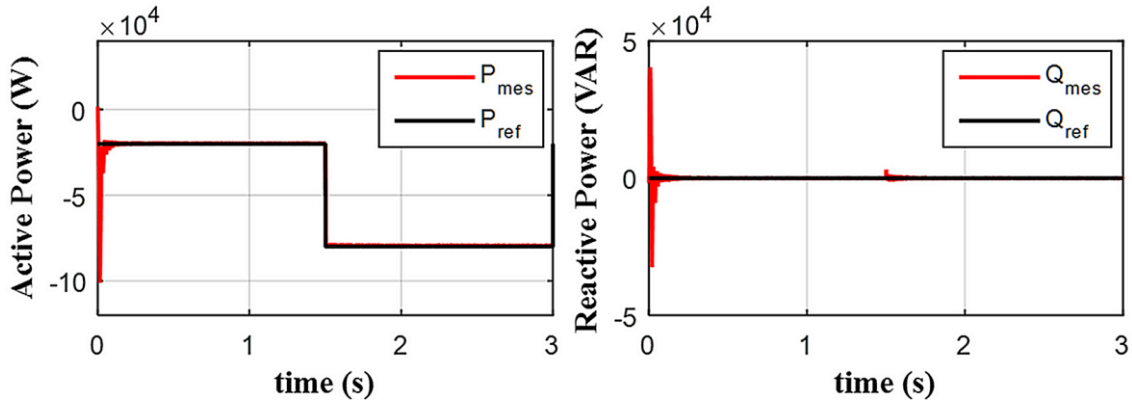

Figure 10. P_G & Q_G powers production regulation with IDA-PBC method

III.3. Discussion

The data presented in Figures 7 and 8 offer significant insights into the accuracy and effectiveness of our frequency tuning model. The graph showcases how the Automatic Frequency Restoration Reserve (aFRR) system efficiently corrects deviations to maintain optimal synchronism at the Kabertene integration point. The red line represents the aFRR-induced error correction, demonstrating its notable impact on enhancing system stability.

In compliance with Algerian regulatory guidelines governing electrical networks, the allowable frequency range spans from 47.5Hz to 48Hz, lasting up to 20 seconds. Our power generation facilities are designed to withstand exceptional conditions within these brief periods. Even amidst rapid frequency fluctuations of up to 1 Hz per second, our electricity production facility maintains synchronization with the transmission network. This design ensures unwavering power supply despite frequency variations, contributing to power system safety and stability. Adhering to these standards and employing effective frequency control measures like aFRR ensures reliable power delivery to consumers. Figures 7 and 8 delineate the operational adaptability facilitated by the aFRR system in managing MW power generation from gas turbines in response to frequency changes. This adaptability aligns gas turbine power generation with the required frequency benchmarks, bolstering power grid stability at the Kabertene integration point.

Frequency control measures, including automatic voltage regulation and reactive power compensation, are crucial for maintaining voltage stability within acceptable thresholds. Figure 9 charts the temporal evolution of voltages within the 220KV transmission and 30KV distribution systems, focusing on the PV injection node. This visual representation offers a comprehensive overview of the influence of photovoltaic integration on voltage levels.

Figure 10 underscores the highest voltage levels at the 220 KV transmission and 30 KV distribution nodes, achieved through the harmonious integration of frequency control measures with renewable energy sources like photovoltaic and wind energy. This graphical depiction provides a comprehensive evaluation of voltage variations during power system operations, serving as a valuable reference for system operators and engineers.

The quantification of operational loss reduction percentages offers enlightening insights into the impact of various factors, including renewable energy integration, optimization techniques, and technical enhancements, on overall system efficacy. This metric aids in evaluating strategies for mitigating energy loss and enhancing system performance. Analyzing data from Tables 1 and Figure 11 enables operators to identify effective techniques for reducing active losses. Regulatory assessments of the Doubly Fed Induction Generator (DFIG) inform decisions on prioritizing interventions for maximum reduction. Active loss reduction measures enhance system efficiency and sustainability, as demonstrated by the pursuit test in Figure 11.

Figure 12 highlights the system's sensitivity to external disturbances during regulatory tests, while Figure 13 underscores the consistent behavior of the DFIG's active and reactive power outputs. Transient endurance tests, depicted in Figures 12 and 13, reveal minimal impact on response time and oscillation amplitude under extreme parameter variations. The state feedback controller effectively manages disturbances, converges to reference trajectories, adheres to MPPT, and recovers from noise or parameter disparities, showcasing its applicability for DFIG-based control.

IV. Conclusion

This study delves into the implementation of diverse control strategies like frequency control, Maximum Power Point Tracking (MPPT), and Particle Swarm Optimization (PSO) to effectively integrate renewable energy sources, particularly Kabertene wind energy, into the autonomous PIAT power grid in Algeria's southern region. The research underscores the efficacy of these methods in boosting grid stability, curbing frequency deviations, and facilitating seamless renewable energy assimilation. Furthermore, the adept administration of dynamic D-ZIP load models through PSO results in reduced active power losses and steady voltage levels across the PIAT grid. The study's culmination offers insights into the practical application of MPPT-PSO algorithms, fostering an eco-friendly energy paradigm. The comparison of Interconnection and Damping-based Control (IDA-PBC) with Synchronous Inner Droop (SIDA-PBC) underscores IDA-PBC's dominance in influencing active power generation, particularly significant for Kabertene's energy production. These findings guide the optimization and integration of renewable energy sources, advancing sustainability and efficiency in the Kabertene region.

Appendix

The parameters used in the model of the DFIG and wind turbine are shown in Table 1:

Table 1. Parameters used in simulation model [3].

Doubly Fed Induction Generators DFIG					
Parameter	Value	Unit	Wind Turbine (WT)		
P_n	100	kW	R	35.25	m
R_s	0.455	Ω	S	π.r2	m2
R_r	0.19	Ω	ρ	1.22	Kg/m3
L_s	0.07	H	G	90	/
L_r	0.0213	H	$J_{turbine}$	1000	Kg/m2
L_m	0.034	H			
J_{DFIG}	0,53	Kg.m²			
f	0,0024	N.m.s/rad			
p	2	/			

References

[1] H. Hamiani, A. Mansouri, A. A. Tadjeddine, A Belaidi, R Salim; "A wind turbine sensorless automatic control systems, analysis, modelling and development of IDA-PBC method ", International Journal of Power Electronics and Drive System (IJPEDS), Vol. 11, No. 1, pp 45~55, March 2020.

[2] W. C. Chen, et al., "Energy stability prediction strategy for polymer electrolyte lithium batteries based upon an improved kinetic programming algorithm", Elsevier Ltd, Energy Reports, Vol. 15, 33 – 37, 2021.

[3] Bahia Kelkoula, Abdelmadjid Boumediene, "Stability analysis and study between Classical Sliding Mode Control (SMC) and Super Twisting Algorithm (STA) for Doubly Fed Induction Generator (DFIG) under Wind turbine", , Elsevier Ltd, Vol. 60, No. 7, pp. 2776-2798, 2020.

[4] A. A. Tadjeddine, R. I. Bendjillali, M. S. Bendelhoum, H. Hamiani, and I. Arbaoui, "Advanced dynamic stability system developed for nonlinear load," International Journal of Power Electronics and Drive Systems (IJPEDS), vol. 14, no. 4, pp. 2031–2042, Dec. 2023. doi:10.11591/ijpeds.v14.i4.pp2031-2042

[5] Jian Xun Jin, Ruo Huan et al., "Combined low voltage ride through and power smoothing control for DFIG/PMSG hybrid wind energy conversion system employing a SMES-based AC-DC unified power quality conditioner ", International Journal of Electrical Power and Energy Systems, 2021.

[6] H. Wen, "Power flow analysis of 110kv power supply system based on PowerWorld," Journal of Physics: Conference Series, vol. 2495, no. 1, p. 012025, 2023. doi:10.1088/1742-6596/2495/1/012025.

[7] A. A. Tadjeddine, M. S. Bendelhoum, R. I. Bendjillali, H. Hamiani, and S. Djelaila, "VRE integrating in Piat grid with AFRR using PSS, MPPT, and PSO-based techniques: A case study kabertene," EAI Endorsed Transactions on Energy Web, vol. 10, 2023. doi:10.4108/ew.3378

[8] Kenneth E. Okedu, Hind F, A. Barghash, "Enhancing the Performance of DFIG Wind Turbines Considering Excitation Parameters of the Insulated Gate Bipolar Transistors and a New PLL Scheme", Frontiers in Energy Research, Vol. 60, No. 7, pp. 2776-2798, 2021.

[9] H. Kai; "Structural Control and Fault Detection of Wind Turbine Systems", Book, Fst Edition IET, 2018.

[10] H. HAMIANI, A. A. Tadjeddine, M. Sekkal, and I. Arbaoui, “Non-linear control by status feedback of the three-phase asynchronous machine,” Algerian Journal of Renewable Energy and Sustainable Development, vol. 5, no. 1, pp. 1–10, 2023. doi:10.46657/ajresd.2023.5.1.1

[11] H. Elaimani, et al., “Adaptive doubly fed induction generator’s control driven wind turbine using Luenberger observer optimized by genetic algorithm,” Indonesian Journal of Electrical Engineering and Computer Science, vol. 29, no. 1, p. 120, 2022. doi:10.11591/ijeecs.v29.i1.pp120-132.

[12] Zhaosen Chai, Hui Li, et al., “Output impedance modeling and grid-connected stability study of virtual synchronous control-based doubly-fed induction generator wind turbines in weak grids”, International Journal of Electrical Power and Energy Systems, 2021.

[13] R. Ortega, and all “Passivity- Based control of Euler Lagrange Systems”, Book, Edition springer, 2013.

[14] Ningsu Luo, Yolanda Vidal and Leonardo Acho; “Advances in Industrial Control, Wind Turbine Control and Monitoring”, Book, Fst Edition springer, 2014.

[15] S. Ebrahimkhani ‘’Robust fractional order sliding mode control of doubly-fed induction generator -based wind turbines ‘’, ISA Transactions, 2016.

[16] S. Mensou, A. Essadki, et al., "Performance of a vector control for DFIG driven by wind turbine: real time simulation using DS1104 controller board," International Journal of Power Electronics and Drive System (IJPEDS), vol. 10(2), pp. 1003-1013, 2019.

[17] Ali Darvish Falehi, Hossein Torkaman; “Promoted supercapacitor control scheme based on robust fractional-order super-twisting sliding mode control for dynamic voltage restorer to enhance FRT and PQ capabilities of DFIG-based wind turbine”, Journal of Energy Storage, 2021.

[18] Hamid Chojaa, Aziz Derouich, Seif Eddine Chehaidia, Othmane Zamzoum, Mohammed Taoussi, Hasnae Elouatouat. ‘’ Integral sliding mode control for DFIG based WECS with MPPT based on artificial neural network under a real wind profile”. Energy Reports, 1, 139–152. 2021.

[19] H. Hamiani, A. A. Tadjeddine, I. Arbaoui, M. S. Bendelhoum, and B. Abdelkrim, “A new robust SIDA-PBC approach to control a DFIG,” Bulletin of Electrical Engineering and Informatics, vol. 12, no. 3, pp. 1310–1317, 2023. doi:10.11591/eei.v12i3.2155.

[20] J. Li, J. Yao, X. Zeng, R. Liu, D. Xu, C. Wang. “Coordinated control strategy for a hybrid wind farm with DFIG and PMSG under symmetrical grid faults.” Energies, 10, 669, 2017.

[21] H. Hamiani, A. A. Tadjeddine, M. Sekkal, et al, “Implementing Non-Linear Control for the Three-Phase Asynchronous Machine via Status Feedback”, AJRESD, vol. 5, no. 01, pp. 1-10, Jun. 2023. Doi:10.46657/ajresd.2023.5.1.1.

[22] N. H. Abdul Kahar et al., “Comparative analysis of grid-connected bifacial and standard mono-facial photovoltaic solar systems,” Bulletin of Electrical Engineering and Informatics, vol. 12, no. 4, pp. 1993–2004, 2023. doi:10.11591/eei.v12i4.5072.

[23] A. Tanvir, A. Merabet, R. Beguenane, “Real-time control of active and reactive power for doubly fed induction generator (DFIG)-based wind energy conversion system”. Energies, 8, 10389–10408. 2015.

[24] A. A. Tadjeddine, “ Electrotechnique fondamentale 1,” vol. Sept. 2023, El-Bayadh, Algeria: Centre Universitaire Nour Bachir El-Bayadh, 2023, pp. 1–127.

[25] F. Oliveira, A. Amorim, L. Encarnação, J. Fardin, Orlando, M. Silva, S. Simonetti, D. “Enhancing LVRT of DFIG by using a superconducting current limiter on rotor circuit “ Energies, 9, 16. 2016.

[26] Sarma, Nur, et al., "Implementation of a conventional DFIG stator flux-oriented control scheme using industrial converters." Renewable Energy Research and Applications (ICRERA), 2016.

[27] I. Lopez-Garcia, G. Espinosa-Perez, H. Siguerdidjane, A. Doria-Cerezo, «On the passivity-based power control of a doubly-fed induction machine". Int. J. Electr. Power Energy Syst., 45, 303–312. 2013.

[28] M. Abdelrahem, C. Hackl and R. Kennel " Sensorless Control of Doubly-Fed Induction Generators in Variable-Speed Wind Turbine Systems in Proceedings", 5th International Conference on Clean Electrical Power (ICCEP) (Taormina) p 406–413. 2015.

[29] A. A. Tadjeddine, I. Arbaoui, A. Harrouz, H. Hamiani, and C. Benoudjafer, “Dispatching and scheduling at Load Peak with the optimal location of the compensation under constraints in real-time,” Algerian Journal of Renewable Energy and Sustainable Development, vol. 2, no. 01, pp. 34–41, 2020. doi:10.46657/ajresd.2020.2.1.5.

[30] Huerta H, Loukianov AG, Cañedo JM. «Passivity sliding mode control for large-scale power systems", IEEE Trans Control Syst Technol. 2018.

[31] Sun H, Aschemann H. «Passivity-based slidingmode control for input-affine nonlinear systems ". Paper presented at: 2016 American Control Conference (ACC), ; Boston, MA. 2016.

[32] A. A. Tadjeddine, Chaker A., Zekkour F., Belaghit A., Hamiani H. “Optimal Intelligent Energy Management to Integrate a Photovoltaic Park into Electricity Grid Using a Real-Time Objective Function—Application to the Naâma Park”, Springer Proceedings in Energy, pp77-84, 2020. https://doi.org/10.1007/978-981-15-5444-5_10.

[33] E. Abderraouf, M. R. Lahcene, M. S. Bendelhoum, S. Zegnoun, A. A. Tadjeddine, and F. Menezla, “Transmission performance in compressed medical images using Turbo Code,” Indonesian Journal of Electrical Engineering and Computer Science, vol. 27, no. 1, p. 318, 2022. doi:10.11591/ijeecs.v27.i1.pp318-327.

[34] R. Othman, “A novel method to improve the power quality via hybrid system,” PRZEGLĄD ELEKTROTECHNICZNY, vol. 1, no. 6, pp. 169–176, 2023. doi:10.15199/48.2023.06.35.

[35] A. A. Tadjeddine, I. Arbaoui, H. Hamiani, and A. Chaker, “Optimal distribution of power under stress on power grid in real-time by reactive compensation-management and development in balance,” International Journal of Power Electronics and Drive Systems (IJPEDS), vol. 11, no. 2, pp. 685–691, 2020. doi:10.11591/ijpeds.v11.i2.pp685-691

[36] Walter Gil-González, Alejandro Garces, Andrés Escobar “Passivity-based control and stability analysis for hydro-turbine governing systems”. Elsevier, 2018.

[37] H. Li, D. Chen, H. Zhang, C. Wu, X. Wang, ‘’ Hamiltonian analysis of a hydro-energy generation system in the transient of sudden load increasing’’, Appl. Energy 185, Part 1, 244–253, 2017.

[38] Montoya, O.D, Gil-González, W. Serra, F.M. ‘’ PBC Approach for SMES Devices in Electric Distribution Networks’’. IEEE Trans. Circuits Syst. II Exp. Briefs, 65, 2003–2007, 2018.

[39] I. Arbaoui, A. A. Tadjeddine, H. Hamiani, and H. Ahmed, “Acoustic study of the influence of climate change on the Propagation of noise generated by industrial units in real-time: by an industrial zone in Algeria,” International Journal of Power Electronics and Drive Systems (IJPEDS), vol. 12, no. 2, p. 1275, 2021. doi:10.11591/ijpeds.v12.i2.pp1275-1282.

[40] L. Bena, M. Nowak, and M. Kusinski, “Analysis of the impact of micro photovoltaic installations on the voltage in the low voltage distribution network,” 2021 Selected Issues of Electrical Engineering and Electronics (WZEE), 2021. doi:10.1109/wzee54157.2021.9577036.

[41] I. Arbaoui, A. Hamou, A. A. Tadjeddine, A. Harrouz, and C. Benoudjafer, “Acoustic study of noise generated by Arzew’s industrial units in limited batteries,” Algerian Journal of Renewable Energy and Sustainable Development, vol. 2, no. 02, pp. 115–125, 2020. doi:10.46657/ajresd.2020.2.2.4.

[42] Van der Schaft, A. L2-Gain and ‘’ Passivity Techniques in Nonlinear Control’’, Springer: Berlin/Heidelberg, Germany, 2017.

[43] Montoya, O.D, Gil-González, W. Avila-Becerril, S. Garces, A. Espinosa-Pérez, G. ‘’ Distributed Energy Resources Integration in AC Grids’’. A Family of Passivity-Based Controll, (in Spanish). Rev. Iberoam. Autom.Inform. Ind., 16, 212–221, 2019.